Magnetoelectric Effect at the Ni/HfO_2 Interface Induced by Ferroelectric Polarization

Qiong Yang,[1,2,*] Lingling Tao,[3] Zhen Jiang,[1] Yichun Zhou,[2] Evgeny Y. Tsymbal,[3,4,†] and Vitaly Alexandrov[1,‡]

[1] *Department of Chemical and Biomolecular Engineering, University of Nebraska, Lincoln, Nebraska 68588, USA*
[2] *School of Materials Science and Engineering, Xiangtan University, Xiangtan, Hunan 411105, China*
[3] *Department of Physics and Astronomy, University of Nebraska, Lincoln, Nebraska 68588, USA*
[4] *Moscow Institute of Physics and Technology, Dolgoprudny, Moscow Region 141700, Russia*

(Received 27 May 2019; revised manuscript received 10 July 2019; published 21 August 2019)

Driven by the technological importance of the recently discovered ferroelectric HfO_2, we explore a magnetoelectric effect at the HfO_2-based ferroelectric-ferromagnetic interface. Using density-functional-theory calculations of the Ni/HfO_2/Ni (001) heterostructure as a model system, we predict a stable and sizable ferroelectric polarization in a few-nm-thick HfO_2 layer. For the Ni/HfO_2 interface with opposite polarization directions (pointing to or away from the interface), we find a sizable difference in the interfacial Ni—O bonding, resulting in dissimilar degrees of depletion of the electron density around the interface. The latter affects the relative population of the exchange-split majority and minority spin bands at the interface and thus the interfacial magnetic moments. The sizable change in the interface magnetization with ferroelectric polarization reversal of HfO_2 manifests a significant ferroelectrically induced magnetoelectric effect at the Ni/HfO_2 interface. Our results reveal promising prospects of ferroelectric-ferromagnetic composite multiferroics based on HfO_2-based ferroelectric materials.

DOI: 10.1103/PhysRevApplied.12.024044

I. INTRODUCTION

Multiferroic materials with coexisting ferroelectric and ferromagnetic orders have attracted much attention due to the magnetoelectric coupling opening alternative prospects for electronic devices [1,2]. Switching magnetization by applied electric rather than magnetic field or spin-polarized current requires much less energy [3–5], making multiferroics promising for memory and logic applications [6,7]. Due to a limited number of single-phase multiferroic compounds operating at room temperature, composite multiferroics containing ferroelectric (or piezoelectric) and ferromagnetic components have been considered as viable candidates [8–11]. It was shown that composite multiferroic materials often have much larger magnetoelectric coupling compared to their single-phase counterparts, resulting from strain-mediated [12–15] or charge-mediated [16–21] coupling mechanisms.

There are, however, a number of challenges to exploiting the magnetoelectric coupling in emerging device technologies [3]. Among them are fabricating multiferroic composite structures at the nanoscale without loss of functionality and making ferroic components compatible with the silicon-based semiconductor technology [22]. It is established that ferroelectric properties often deteriorate with reducing film thickness, which makes a composite structure useless at the nanoscale. Also, most of the traditional perovskite ferroelectrics are incompatible with the CMOS technology.

Recently, ferroelectricity has been discovered in doped hafnia (HfO_2) films [23,24], which may help to address the abovementioned challenges. The origin of the ferroelectric behavior was attributed to the formation of a noncentrosymmetric orthorhombic phase of HfO_2. First-principles calculations predicted two possible ferroelectric phases of HfO_2, namely, orthorhombic polar phases with the space group symmetries of $Pca2_1$ and $Pmn2_1$ [25]. The direct experimental evidence of the ferroelectric $Pca2_1$ phase was provided by scanning transmission electron microscopy [26]. These findings stimulated significant efforts in studying relevant properties of ferroelectric HfO_2 films [27–32], showing their applicability as a functional gate oxide in nanoscale FeFET memory devices [33,34] and ferroelectric tunnel junctions [35–37].

These results indicate that ferroelectric HfO_2 may be a promising material to serve as a ferroelectric component in composite multiferroic structures. Due to the ferroelectricity of doped HfO_2 thin films down to a few nanometers

*qyang@xtu.edu.cn
†tsymbal@unl.edu
‡valexandrov2@unl.edu

thickness [38] and good compatibility with the Si-based semiconductor process [39], HfO_2-based multiferroic heterostructures are potentially feasible for technological applications. In this regard, exploring the magnetoelectric effect in ferroelectric and ferromagnetic heterostructures where HfO_2 is used as a ferroelectric constituent is important for searching alternate composite multiferroics compatible with Si technology.

In this paper, we employ density functional theory (DFT) calculations to explore the charge-mediated magnetoelectric coupling between ferroelectric HfO_2 and ferromagnetic Ni thin films, which is also compatible with the Si-based semiconductor technology [40,41], in a composite multiferroic layered structure. We assume that HfO_2 belongs to the orthorhombic structural phase of the $Pca2_1$ space group with the polarization direction perpendicular to the interface and consider fcc Ni as a representative ferromagnetic metal film to create a $Ni/HfO_2/Ni$ (001) ferroelectric-ferromagnetic heterostructure. We demonstrate a stable and switchable ferroelectric polarization in the heterostructured HfO_2 thin films and predict a strong magnetoelectric coupling at the Ni/HfO_2 interface driven by HfO_2 polarization reversal. Our results provide additional insights into the ferroelectricity of HfO_2 thin films and mechanisms of the magnetoelectric coupling induced by polarization switching. These insights may be useful for the experimental realization of composite multiferroic materials based on ferroelectric HfO_2.

II. COMPUTATIONAL METHODOLOGY

DFT calculations are performed using the Vienna *Ab initio* simulation package (VASP) within the projector-augmented wave (PAW) formalism [42]. The generalized gradient approximation Perdew-Burke-Ernzerhof (GGA PBE) functional [43] is adopted to treat the exchange-correlation effects. The optimized lattice constant of Ni along the (110) direction is found to be 4.980 Å, which is only 0.1% less than the experimental lattice constant (4.984 Å). The optimized lattice parameters *a*, *b,* and *c* of the orthorhombic unit cell of HfO_2 ($Pca2_1$ space group) are 5.246, 5.034, and 5.064 Å, respectively, in good agreement with the experimental data [26] and the previous DFT results [44,45]. The spontaneous polarization for bulk HfO_2 calculated using the Berry phase method [46] is 51.8 $\mu C/cm^2$, which agrees well with previously reported theoretical and experimental values [21,28,47]. The calculated band gap of the bulk HfO_2 is 4.36 eV, which is in reasonable agreement with the experimentally measured value (5.6 eV) [48]. It should be mentioned that the hybrid exchange-correlation functionals could provide a better agreement between theoretical and experimental band gaps [49,50], however, at a much higher computational cost.

To explore the magnetoelectric properties of the Ni/HfO_2 interfaces, we construct $Ni/HfO_2/Ni$ heterostructures by stacking N unit cell (u.c.) layers of HfO_2 and nine monolayers of Ni along the (001) direction. We assume symmetric interface terminations, which allows us to examine the magnetic properties of the Ni/HfO_2 (001) interface for polarization pointing to the Ni layer ($P_\downarrow$) or away from the Ni layer ($P_\uparrow$), using the same structural model with unidirectional polarization of HfO_2. We note that, since the conventional unit cell of HfO_2 contains four Hf and eight O atoms arranged in alternating atomic planes of Hf and O, such a nonstoichiometric HfO_2 slab has a noninteger number of unit cells N. The convergence of interfacial polarization and magnetization with respect to HfO_2 thickness is analyzed by constructing heterostructures with three different thicknesses of the HfO_2 layer (Fig. 1). Specifically, the number of considered HfO_2 layers N is set to 3.75, 4.75, and 5.75 to create the O/Ni terminations at both interfaces (since one u.c. layer of HfO_2 contains four alternating atomic planes of Hf and O, 0.25 u.c. layer represents one Hf or one O atomic plane), which is more energetically favorable. For studying the magnetoelectric effect, we consider the $Ni/HfO_2/Ni$ heterostructure with HfO_2 thickness $N = 4.75$. A $6 \times 6 \times 1$ Monkhorst-Pack k-point mesh [51] is used for Brillouin zone integration.

By comparing the total energies of the $Ni/HfO_2/Ni$ heterostructures with O atoms locating at the hollow and atop sites of the interfacial Ni atoms, we find that the hollow-site configuration is about 0.7 eV energetically more favorable than the atop configuration. Therefore, in this work, we only focus on the hollow-site configuration

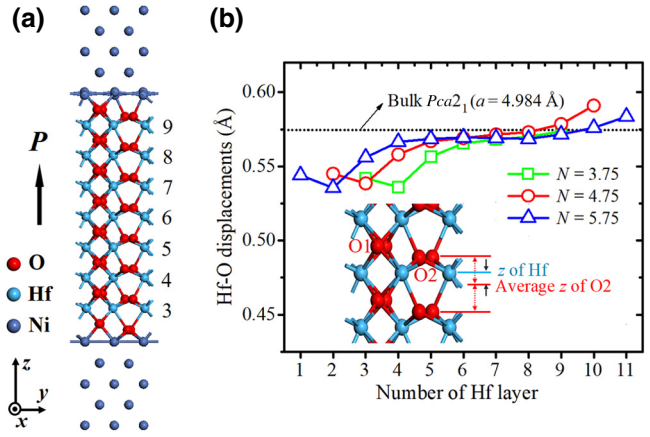

FIG. 1. (a) The atomic structure of the ferroelectric $Ni/HfO_2/Ni$ heterostructure ($N = 3.75$). (b) Polar displacements across the HfO_2 layer are in $Ni/HfO_2/Ni$ heterostructures for $N = 3.75$, 4.75, and 5.75. The numbers, increasing along the polarization direction, denote Hf atomic layers. The horizontal dotted line denotes the Hf-O displacement for the bulk $Pca2_1$ HfO_2 with $a = b = 4.984$ Å. Inset: method to quantify the Hf-O polarization displacement, which is defined as the difference between the z coordinate of the Hf plane and the averaged z coordinate of the two adjacent O2 planes.

of the Ni/HfO_2 interfaces as shown in Fig. 1(a). The in-plane lattice constant of the heterostructure is fixed to the experimental value of cubic Ni (4.984 Å), while the out-of-plane lattice constant and all the internal coordinates are fully relaxed. Under this constraint, polarization of bulk HfO_2 is enhanced up to 64.7 $\mu C/cm^2$. The effect of strain on the magnetoelectric effect is also analyzed (see the Supplemental Material [52]) by constraining the in-plane lattice constant to the experimental value of yttrium-stabilized zirconia (YSZ, $a = 5.185$ Å) [53], which is a commonly used substrate in the epitaxial growth of HfO_2-based ferroelectric films.

III. RESULTS AND DISCUSSION

Figure 1(a) depicts the employed structural model of the Ni/HfO_2/Ni heterostructure. Figure 1(b) shows the calculated relative displacements between hafnium and oxygen atoms across the HfO_2 layer. From the inset of Fig. 1(b), it is seen that there are two types of symmetrically inequivalent oxygen atoms in the $Pca2_1HfO_2$: the oxygen (denoted as O1), which is located in the central plane of the two adjacent Hf atomic planes and the oxygen (denoted as O2), which is displaced along the $-z$ direction from the central plane leading to the ferroelectric polarization along $+z$ direction. Therefore, we define the polar Hf-O displacement in the HfO_2 layer as the difference between the z coordinate of each Hf atomic layer and average z coordinate of the two adjacent O2 atomic planes as illustrated by the insert in Fig. 1(b). It can be seen that the polar displacements are not uniform across the HfO_2 layer with displacements being reduced (increased) near the bottom (top) interface. In general, the displacement profiles for the heterostructures with different thicknesses of HfO_2 reveal similar features, and the displacement in the central HfO_2 layers is close to that for the bulk HfO_2 (0.57 Å). The observed magnitude of polar displacements is rather large as compared to the Ti-O polar displacements in typical perovskite ferroelectrics such as $PbTiO_3$ (0.32 Å) [54]. Such a Hf-O displacement profile in the HfO_2 layer results in shorter (longer) Ni—O2 bonds at the bottom (top) interfaces for polarization pointing along the $+z$ direction. We can also notice some increase in the Hf-O displacement near the bottom interface (see Fig. 1) due to a strong Ni-O2 interaction that weakens the bonds between Hf and O2 atoms.

Next, we analyze the atomic structure around the Ni/HfO_2 interfaces, which are different by polarization orientation pointing away from ($P_\uparrow$) and to ($P_\downarrow$) the interface. Figures 2(a) and 2(b) show the side views of the two interfaces. It is seen that the main difference between the atomic structures at the $P_\uparrow$ and $P_\downarrow$ interfaces results from the displacements of the O2 atoms leading to contraction and elongation of the Ni—O2 bonds at the two interfaces, respectively. Figures 2(c) and 2(d) show the top views of

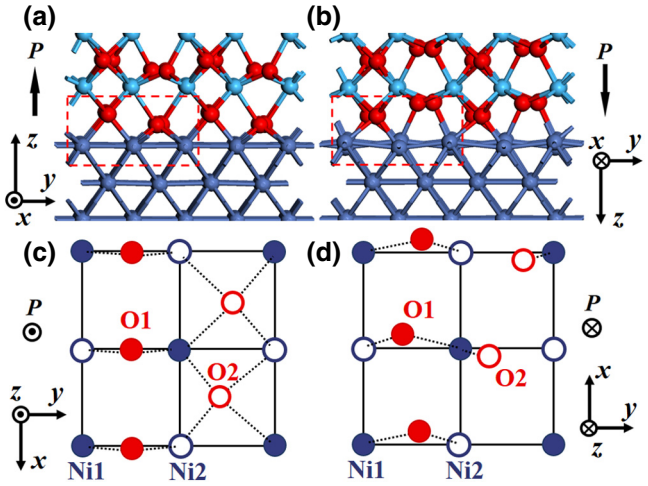

FIG. 2. Side views of atomic structures of the Ni/HfO_2 interface with polarization pointing away from (a) or to (b) the Ni layer. (c),(d): Top views of the same interfaces, where only the two atomic layers at the interfaces denoted by the red dashed frames in (a),(b) are shown.

the corresponding Ni/HfO_2 interfaces. It is seen that the O1 atoms are located at the bridge sites between Ni atoms at both interfaces, while the positions of the O2 atoms are different. At the $P_\uparrow$ interface, O2 atoms are located at the hollow position surrounded by four interfacial Ni atoms, resulting in the Ni—O2 bond lengths of 1.973, 1.977, 2.062, and 2.127 Å. At the $P_\downarrow$ interface, however, the Ni—O2 bond distances are larger (2.012 and 2.639 Å for the two nearest Ni atoms), suggesting much weaker Ni-O2 interactions than those at the $P_\downarrow$ interface. Due to the difference between the Ni-O interactions at both interfaces, the atomic and electron structures of the interfacial Ni atoms are not equivalent and are distinguished by using notations of Ni1 and Ni2, respectively.

The calculated magnetic moments (μ) of the Ni and O interfacial atoms are listed in Table I. It is seen that they differ considerably for the two polarization states of the HfO_2 film (pointing away from or to the Ni layer). For example, two Ni atoms at the $P_\uparrow$ interface exhibit magnetic moments of 1.088 and 1.068 μ_B, more than 0.2 μ_B larger than those of the Ni atoms at the $P_\downarrow$ interface. The O1 atoms at the two interfaces, which exhibit very small displacements upon polarization switching, have comparable magnetic moments. However, magnetic moments of the O2 atoms at the two interfaces differ substantially ($\Delta\mu = 0.254$ μ_B), which is consistent with the different Ni—O2 bond lengths at the two interfaces. Therefore, the polarization-induced difference between the total magnetic moments at the two interfaces reaches 1.448 μ_B (0.058 $\mu_B/Å^2$), which is significantly larger than that of the Fe/$BaTiO_3$ interfaces (0.019 $\mu_B/Å^2$) [16]. We point out that all the magnetic moments of the aforementioned Ni and O atoms at both interfaces are significantly larger than

TABLE I. The magnetic moments (in μ_B) of selected interfacial atoms shown in Figs. 2(c) and 2(d) for the $P_\uparrow$ [$\mu(P_\uparrow)$] and $P_\downarrow$ [$\mu(P_\downarrow)$] interfaces.

Atom	$\mu\,(P_\uparrow)$	$\mu\,(P_\downarrow)$	$\Delta\mu$
Ni1	1.088	0.888	0.200
Ni2	1.068	0.820	0.248
O1	0.184	0.142	0.042
O2	0.337	0.083	0.254
Total	5.353	3.865	1.488

$\Delta\mu$ is the difference between the atomic magnetic moments at the two interfaces. Total magnetic moments in the last row are counted in an interface unit cell, which includes 2 Ni1, 2 Ni2, 2 O1 and 2 O2 at each interface. The magnetic moments for the unlisted atoms of the heterostructure are almost zero for HfO_2 and close to the bulk values for Ni.

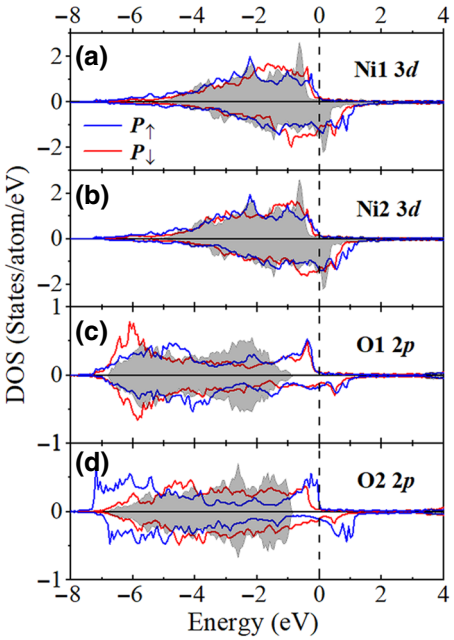

FIG. 3. Orbital-resolved DOS for interfacial atoms of ferroelectric $Ni/HfO_2/Ni$ heterostructure: (a) 3*d* of Ni1, (b) 3*d* of Ni2, (c) 2*p* of O1, and (d) 2*p* of O2. The majority and minority spin DOS are plotted upward (positive) and downward (negative), respectively. The blue and red lines denote DOS of atoms at the $P_\uparrow$ and $P_\downarrow$ interfaces, respectively. The gray-filled curves represent the DOS of atoms in the central atomic layers, which are close to the bulk atoms. The vertical dashed line indicates the position of Fermi energy.

those of the Ni (0.623 μ_B) and O (0 μ_B) atoms in the bulk Ni and HfO_2. For a comparison, we have also calculated interfacial magnetization of the nonferroelectric Ni/HfO_2 (*Fm*3*m*)/Ni heterostructure by imposing mirror symmetry with the central Hf atomic layer, as shown in the Supplemental Material [52]. The average magnetic moments of interfacial Ni and O in the nonferroelectric $Ni/HfO_2/Ni$ heterostructure are 0.994 and 0.200 μ_B, which are nearly the average values of the magnetic moments of Ni and O at the $P_\uparrow$ and $P_\downarrow$ interfaces.

To understand the origin of the polarization-induced difference in magnetization at the Ni/HfO_2 interface, we further analyze the electronic properties of the interfacial structures in terms of local density of states (DOS). Figure 3 shows the local DOS projected onto the Ni 3*d* and O 2*p* electronic states of the interfacial atoms. The overall trend is that the DOS of all the interfacial Ni and O atoms moves to the higher energy relative to the bulk DOS, especially in the case of O atoms. This is due to the interfacial O atoms attracting electron density from the nearby Ni atoms to saturate the broken bonds with Hf at the Ni/HfO_2 interface. Since the minority spin DOS at the Fermi energy is much larger than the majority spin DOS, the loss of the minority spin electrons leads to the increase of magnetic moments of the interfacial Ni compared to the bulk Ni. Hybridization between the Ni 3*d* and O 2*p* orbitals at the interface (seen in Fig. 3 from the O 2*p* DOS mirroring the Ni 3*d* DOS around the Fermi energy) leads to the exchange splitting of the O 2*p* bands, inducing magnetic moments on the O1 and O2 atoms. A similar behavior is also observed in the nonferroelectric $Ni/HfO_2/Ni$ heterostructures, as shown in the Supplemental Material [52], indicating that the overall enhanced magnetism at the Ni/HfO_2 interface is independent of the ferroelectric polarization. Ferroelectric polarization changes the electron occupation and the strength of hybridization between the Ni 3*d* and O 2*p* orbitals at the interface and affects the magnitude of the magnetic moments on the interfacial Ni and O atoms as discussed below.

For the ferroelectric $Ni/HfO_2/Ni$ heterostructure, as seen from Figs. 3(a) and 3(b), the Ni 3*d* DOS at the $P_\uparrow$ interface shifts to the higher energy compared to the Ni 3*d* DOS at the $P_\downarrow$ interface. This is due to the positive (negative) screening charge at the $P_\uparrow$ ($P_\downarrow$) interface, which leads to the enhanced (suppressed) depletion of minority spin electrons and hence to the enhanced (reduced) magnetic moments of the interfacial Ni atoms. This behavior is mirrored by the interfacial O atoms. As seen from Figs. 3(c) and 3(d), the enhanced (reduced) depletion of minority spin electrons occurs at the interfacial O 2*p* orbitals, which enhances (reduces) the magnetic moments of the O atoms at the $P_\uparrow$ ($P_\downarrow$) interface. The effect is especially sizable for the O2 atoms at the $P_\uparrow$ interface, due to the strong Ni—O2 bonding described above. The strong hybridization between the Ni 3*d* and O2 2*p* orbitals at the $P_\uparrow$ interface leads to the large asymmetry between the spin-up and spin-down DOS of the O2 2*p* states, as can be seen from the spin-resolved DOS in Fig. 3(d). This results in the notable difference in the magnetic moments of the O2 atoms at the two interfaces (0.254 μ_B).

Based on the above observations, we conclude that the ferroelectrically induced magnetoelectric effect at the

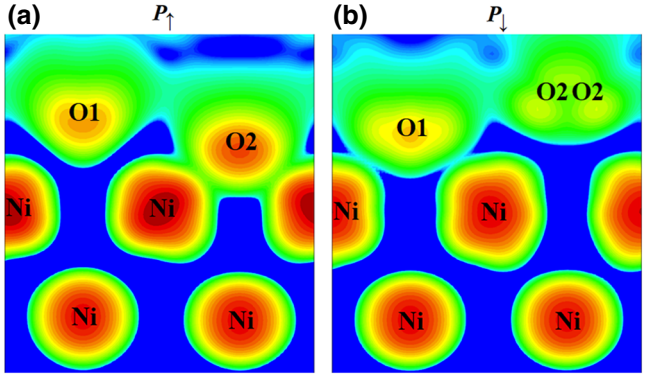

FIG. 4. Spin densities, defined as the difference between the majority and minority spin charge densities, at the $P_\uparrow$ (a) and $P_\downarrow$ (b) interfaces, respectively. The spin densities are shown within the *y*-*z* plane by averaging the spin densities along the *x* direction for the convenience of demonstration.

Ni/HfO_2 interface can be attributed to two main effects: (1) the larger (smaller) electron density depletion at the $P_\uparrow$ ($P_\downarrow$) interface due to screening of the polarization charge of ferroelectric HfO_2, and (2) the stronger (weaker) hybridization between the O 2*p* and Ni 3*d* orbitals at the $P_\uparrow$ ($P_\downarrow$) interface due to the shorter (longer) Ni—O bonds induced by polarization.

The difference in magnetization between the $P_\uparrow$ and $P_\downarrow$ interfaces due to ferroelectric polarization of HfO_2 is further illustrated by plotting spin densities at both interfaces (Fig. 4). It is seen from Fig. 4(a) that the O2 atoms have stronger interaction with the interfacial Ni atoms when polarization is pointing away from Ni. It induces more significant magnetization of O2 at the $P_\uparrow$ interface [Fig. 4(a)] compared to that at the $P_\downarrow$ interface as shown in Fig. 4(b). The larger depletion of electron density at the $P_\uparrow$ interface, which is the loss of minority spin electrons as shown by the orbital-resolved DOS of the interfacial atoms in Fig. 3, contributes to the larger spin density at the $P_\uparrow$ interface than at the other interface.

IV. CONCLUSIONS

To summarize, we study ferroelectricity and the magnetoelectric effects in Ni/HfO_2/Ni (001) heterostructures by means of DFT calculations. We find that a stable and switchable ferroelectric polarization is sustained in the HfO_2 films of a few unit cells. Reversal of the polarization leads to a sizeable change in the interfacial magnetic moments at the Ni/HfO_2 interface, which manifests an interface magnetoelectric effect induced by ferroelectric polarization. This magnetoelectric effect originates from stronger (weaker) Ni-O interactions and the higher (lower) depletion of minority spin electrons when the polarization direction is pointing away from (to) the ferromagnetic Ni layer. This mechanism of the ferroelectrically induced magnetoelectric effect is of general significance, and therefore, we expect a similar behavior for interfaces between HfO_2-based ferroelectrics and other ferromagnetic metals, such as Fe, Co, and their alloys. Since HfO_2-based thin films sustain a stable ferroelectric polarization at a very small film thickness and are compatible with Si-based semiconductor technology, our findings have potential for applications in microelectronics. We hope, therefore, that our theoretical predictions of a large magnetoelectric effect at the Ni/HfO_2 interface will stimulate experimental studies of this and other composite multiferroics based on ferroelectric HfO_2.

ACKNOWLEDGMENTS

This work was supported by the National Science Foundation (NSF) through MRSEC (Grant No. DMR-1420645) and EPMD (Grant No. ECCS-1917635) Programs and the Russian Science Foundation (Grant No. 18-12-00434). Q. Yang thanks the China Scholarship Council (CSC) for financial support.

[1] W. Eerenstein, N. Mathur, and J. F. Scott, Multiferroic and magnetoelectric materials, Nature **442**, 759 (2006).
[2] N. A. Spaldin and R. Ramesh, Advances in magnetoelectric multiferroics, Nat. Mater. **18**, 203 (2019).
[3] E. Y. Tsymbal, Spintronics: Electric toggling of magnets, Nat. Mater. **11**, 12 (2012).
[4] S. Manipatruni, D. E. Nikonov, and I. A. Young, Beyond CMOS computing with spin and polarization, Nat. Phys. **14**, 338 (2018).
[5] P. B. Meisenheimer, S. Novakov, N. M. Vu, and J. T. Heron, Perspective: Magnetoelectric switching in thin film multiferroic heterostructures, J. Appl. Phys. **123**, 240901 (2018).
[6] J. F. Scott, Data storage: Multiferroic memories, Nat. Mater. **6**, 256 (2007).
[7] M. Bibes and A. Barthélémy, Multiferroics: Towards a magnetoelectric memory, Nat. Mater. **7**, 425 (2008).
[8] L. W. Martin, S. P. Crane, Y.-H. Chu, M. B. Holcomb, M. Gajek, M. Huijben, C.-H. Yang, N. Balke, and R. Ramesh, Multiferroics and magnetoelectrics: Thin films and nanostructures, J. Phys.: Condens. Matter **20**, 434220 (2008).
[9] J. P. Velev, S. S. Jaswal, and E. Y. Tsymbal, Multiferroic and magnetoelectric materials and interfaces, Philos. Trans. R. Soc., A **369**, 3069 (2011).
[10] C. A. F. Vaz, Electric field control of magnetism in multiferroic heterostructures, J. Phys.: Condens. Matter **24**, 333201 (2012).
[11] J.-M. Hu, C.-G. Duan, C.-W. Nan, and L.-Q. Chen, Understanding and designing magnetoelectric heterostructures guided by computation: Progresses, remaining questions, and perspectives, npj Comp. Mater. **3**, 18 (2017).
[12] C.-W. Nan, M. I. Bichurin, S. Dong, D. Viehland, and G. Srinivasan, Multiferroic magnetoelectric composites:

Historical perspective, status, and future directions, J. Appl. Phys. **103**, 031101 (2008).

[13] T. X. Nan, Z. Y. Zhou, J. Lou, M. Liu, X. Yang, Y. Gao, S. Rand, and N. X. Sun, Voltage impulse induced bistable magnetization switching in multiferroic heterostructures, Appl. Phys. Lett. **100**, 132409 (2012).

[14] K. J. A. Franke, D. López González, S. J. Hämäläinen, and S. van Dijken, Size Dependence of Domain Pattern Transfer in Multiferroic Heterostructures, Phys. Rev. Lett. **112**, 017201 (2014).

[15] Q. Wang, X. Li, C.-Y. Liang, A. Barra, J. Domann, C. Lynch, A. Sepulveda, and G. Carman, Strain-mediated 180° switching in CoFeB and Terfenol-D nanodots with perpendicular magnetic anisotropy, Appl. Phys. Lett. **110**, 102903 (2017).

[16] C. G. Duan, S. S. Jaswal, and E. Y. Tsymbal, Predicted Magnetoelectric Effect in Fe/$BaTiO_3$ Multilayers: Ferroelectric Control of Magnetism, Phys. Rev. Lett. **97**, 047201 (2006).

[17] K. Yamauchi, B. Sanyal, and S. Picozzi, Interface effects at a half-metal/ferroelectric junction, Appl. Phys. Lett. **91**, 062506 (2007).

[18] H. J. A. Molegraaf, J. Hoffman, C. A. F. Vaz, S. Gariglio, D. van der Marel, C. H. Ahn, and J.-M. Triscone, Magnetoelectric effects in complex oxides with competing ground states, Adv. Mater. **21**, 3470 (2009).

[19] G. Radaelli, D. Petti, E. Plekhanov, I. Fina, P. Torelli, B. R. Salles, M. Cantoni, C. Rinaldi, D. Gutiérrez, G. Panaccione, M. Varela, S. Picozzi, J. Fontcuberta, and R. Bertacco, Electric control of magnetism at the Fe/$BaTiO_3$ interface, Nat. Commun. **5**, 3404 (2014).

[20] Z. Zhou, B. M. Howe, M. Liu, T. Nan, X. Chen, K. Mahalingam, N. X. Sun, and G. J. Brown, Interfacial charge-mediated non-volatile magnetoelectric coupling in $Co_{0.3}Fe_{0.7}/Ba_{0.6}Sr_{0.4}TiO_3/Nb:SrTiO_3$ multiferroic heterostructures, Sci. Rep. **5**, 7740 (2015).

[21] A. Rajapitamahuni, L. L. Tao, Y. Hao, J. Song, X. Xu, E. Y. Tsymbal, and X. Hong, Ferroelectric polarization control of magnetic anisotropy in $Pb(Zr_{0.2}Ti_{0.8})O_3/La_{0.8}Sr_{0.2}MnO_3$ multiferroic heterostructures, Phys. Rev. Mater. **3**, 021401 (2019).

[22] M. M. Vopson, Fundamentals of multiferroic materials and their possible applications, Crit. Rev. Solid State **40**, 223 (2015).

[23] T. S. Böscke, J. Müller, D. Bräuhaus, U. Schröder, and U. Böttger, Ferroelectricity in hafnium oxide thin films, Appl. Phys. Lett. **99**, 102903 (2011).

[24] J. Müller, T. S. Böscke, U. Schröder, S. Mueller, D. Bräuhaus, U. Böttger, L. Frey, and T. Mikolajick, Ferroelectricity in simple binary ZrO_2 and HfO_2, Nano Lett. **12**, 4318 (2012).

[25] T. D. Huan, V. Sharma, G. A. Rossetti, Jr., and R. Ramprasad, Pathways towards ferroelectricity in hafnia, Phys. Rev. B **90**, 064111 (2014).

[26] X. Sang, E. D. Grimley, T. Schenk, U. Schroeder, and J. M. LeBeau, On the structural origins of ferroelectricity in HfO_2 thin films, Appl. Phys. Lett. **106**, 162905 (2015).

[27] D. Zhou, J. Müller, J. Xu, S. Knebel, D. Brauhaus, and U. Schröder, Insights into electrical characteristics of silicon doped hafnium oxide ferroelectric thin films, Appl. Phys. Lett. **100**, 082905 (2012).

[28] S. Clima, D. J. Wouters, C. Adelmann, T. Schenk, U. Schröder, M. Jurczak, and G. Pourtois, Identification of the ferroelectric switching process and dopant-dependent switching properties in orthorhombic HfO_2: A first principles insight, Appl. Phys. Lett. **104**, 092906 (2014).

[29] D. Martin, J. Müller, T. Schenk, T. M. Arruda, A. Kumar, E. Strelcov, E. Yurchuk, S. Müller, D. Pohl, and U. Schröder, Ferroelectricity in Si-doped HfO_2 revealed: A binary lead-free ferroelectric, Adv. Mater. **26**, 8198 (2014).

[30] S. Zarubin, E. Suvorova, M. Spiridonov, D. Negrov, A. Chernikova, A. Markeev, and A. Zenkevich, Fully ALD-grown $TiN/Hf_{0.5}Zr_{0.5}O_2/TiN$ stacks: Ferroelectric and structural properties, Appl. Phys. Lett. **109**, 192903 (2016).

[31] L. L. Tao, T. R. Paudel, A. A. Kovalev, and E. Y. Tsymbal, Reversible spin texture in ferroelectric HfO_2, Phys. Rev. B **95**, 245141 (2017).

[32] T. Shimizu, T. Mimura, T. Kiguchi, T. Shiraishi, T. Konno, Y. Katsuya, O. Sakata, and H. Funakubo, Ferroelectricity mediated by ferroelastic domain switching in HfO_2-based epitaxial thin films, Appl. Phys. Lett. **113**, 212901 (2018).

[33] S. Mueller, J. Müller, R. Hoffmann, E. Yurchuk, T. Schlösser, R. Boschke, J. Paul, M. Goldbach, T. Herrmann, A. Zaka, U. Schröder, and T. Mikolajick, From MFM capacitors toward ferroelectric transistors: Endurance and disturb characteristics of HfO_2-based FeFET devices, IEEE Trans. Electron Dev. **60**, 4199 (2013).

[34] M. Seo, M.-H. Kang, S.-B. Jeon, H. Bae, J. Hur, B. C. Jang, S. Yun, S. Cho, W.-K. Kim, M.-S. Kim, K.-M. Hwang, S. Hong, S.-Y. Choi, and Y.-K. Choi, First demonstration of a logic-process compatible junctionless ferroelectric Fin-FET synapse for neuromorphic applications, IEEE Electron Device Lett. **39**, 1445 (2018).

[35] F. Ambriz-Vargas, G. Kolhatkar, M. Broyer, A. Hadj-Youssef, R. Nouar, A. Sarkissian, R. Thomas, C. Gomez-Yáñez, M. A. Gauthier, and A. Ruediger, A complementary metal oxide semiconductor process-compatible ferroelectric tunnel junction, ACS Appl. Mater. Interfaces **9**, 13262 (2017).

[36] A. Chouprik, A. Chernikova, A. Markeev, V. Mikheev, D. Negrov, M. Spiridonov, S. Zarubin, and A. Zenkevich, Electron transport across ultrathin ferroelectric $Hf_{0.5}Zr_{0.5}O_2$ films on Si, Microelectron. Eng. **178**, 250 (2017).

[37] Y. Goh and S. Jeon, Enhanced tunneling electroresistance effects in HfZrO-based ferroelectric tunnel junctions by high-pressure nitrogen annealing, Appl. Phys. Lett. **113**, 052905 (2018).

[38] X. Tian, S. Shibayama, T. Nishimura, T. Yajima, S. Migita, and A. Toriumi, Evolution of ferroelectric HfO_2 in ultrathin region down to 3 nm, Appl. Phys. Lett. **112**, 102902 (2018).

[39] A. Chernikova, M. Kozodaev, A. Markeev, D. Negrov, M. Spiridonov, S. Zarubin, O. Bak, P. Buragohain, H. Lu, E. Suvorova, A. Gruverman, and A. Zenkevich, Ultrathin $Hf_{0.5}Zr_{0.5}O_2$ ferroelectric films on Si, ACS Appl. Mater. Interfaces **8**, 7232 (2016).

[40] J. A. Kittl, A. Lauwers, O. Chamirian, M. Van Dal, A. Akheyar, M. De Potter, R. Lindsay, and K. Maex, Ni- and Co-based silicides for advanced CMOS applications, Microelectron. Eng. **70**, 158 (2003).

[41] J. Kim and W. A. Anderson, Direct electrical measurement of the self-assembled nickel silicide nanowire, Nano Lett. **6**, 1356 (2006).

[42] G. Kresse and D. Joubert, From ultrasoft pseudopotentials to the projector augmented-wave method, Phys. Rev. B **59**, 1758 (1999).

[43] J. P. Perdew, K. Burke, and M. Ernzerhof, Generalized Gradient Approximation Made Simple, Phys. Rev. Lett. **77**, 3865 (1996).

[44] R. Materlik, C. Künneth, and A. Kersch, The origin of ferroelectricity in $Hf_{1-x}Zr_xO_2$: A computational investigation and a surface energy model, J. Appl. Phys. **117**, 134109 (2015).

[45] R. Batra, T. D. Huan, J. L. Jones, G. Rossetti Jr, and R. Ramprasad, Factors favoring ferroelectricity in hafnia: A first-principles computational study, J. Phys. Chem. C **121**, 4139 (2017).

[46] R. King-Smith and D. Vanderbilt, Theory of polarization of crystalline solids, Phys. Rev. B **47**, 1651 (1993).

[47] T. Shimizu, K. Katayama, T. Kiguchi, A. Akama, T. J. Konno, O. Sakata, and H. Funakubo, The demonstration of significant ferroelectricity in epitaxial Y-doped HfO_2 film, Sci. Rep. **6**, 32931 (2016).

[48] V. V. Afanas'ev, A. Stesmans, F. Chen, X. Shi, and S. A. Campbell, Internal photoemission of electrons and holes from (100)Si into HfO_2, Appl. Phys. Lett. **81**, 1053 (2002).

[49] R. I. Eglitis and A. I. Popov, Systematic trends in (0 0 1) surface ab initio calculations of ABO3 perovskites, J. Saudi Chem. Soc. **22**, 459 (2018).

[50] R. I. Eglitis, Ab initio calculations of the atomic and electronic structure of $BaZrO_3$ (111) surfaces, Solid State Ionics **230**, 43 (2013).

[51] H. J. Monkhorst and J. D. Pack, Special points for Brillouin-zone integrations, Phys. Rev. B **13**, 5188 (1976).

[52] See Supplemental Material at http://link.aps.org/supplemental/10.1103/PhysRevApplied.12.024044 for the interfacial magnetization and magnetoelectric effect of the strained Ni/HfO_2/Ni heterostructure and the nonferroelectric Ni/HfO_2/Ni heterostructure.

[53] K. Katayama, T. Shimizu, O. Sakata, T. Shiraishi, S. Nakamura, T. Kiguchi, A. Akama, T. J. Konno, H. Uchida, and H. Funakubo, Orientation control and domain structure analysis of {100}-oriented epitaxial ferroelectric orthorhombic HfO_2-based thin films, J. Appl. Phys. **119**, 134101 (2016).

[54] A. M. Glazer and S. A. Mabud, Powder profile refinement of lead zirconate titanate at several temperatures. II. Pure $PbTiO_3$, Acta Cryst. **34**, 1065 (1978).